ADVANCING EARTH AND SPACE SCIENCE

Geophysical Research Letters

RESEARCH LETTER
10.1029/2021GL096304

Key Points:
- Gradient method using Global Positioning System radio occultation data overestimates boundary layer height when multilocal minimum refractivity gradients exist
- This issue is addressed by combining the original method with lifting condensation level (LCL) in the derivation of boundary layer height
- The above deficiency for summer daytime boundary layer height is largely reduced over land for LCL < 2 km, usually over humid regions

Supporting Information:

Supporting Information may be found in the online version of this article.

Correspondence to:

Y. Wang and X. Xu,
pbl_wyj@sina.cn;
xuxd@cma.gov.cn

Citation:

Wang, Y., Zeng, X., Xu, X., Xie, F., & Zhao, Y. (2022). Improving the estimate of summer daytime planetary boundary layer height over land from GPS radio occultation data. *Geophysical Research Letters*, *49*, e2021GL096304. https://doi.org/10.1029/2021GL096304

Received 23 SEP 2021
Accepted 22 DEC 2021

Improving the Estimate of Summer Daytime Planetary Boundary Layer Height Over Land From GPS Radio Occultation Data

Yinjun Wang[1,2], Xubin Zeng[2], Xiangde Xu[1], Feiqin Xie[3], and Yang Zhao[1]

[1]State Key Laboratory of Severe Weather, Chinese Academy of Meteorological Sciences, Beijing, China, [2]Department of Hydrology and Atmospheric Sciences, University of Arizona, Tucson, AZ, USA, [3]Department of Physical and Environmental Sciences, Texas A&M University-Corpus Christi, Corpus Christi, TX, USA

Abstract Global Positioning System (GPS) radio occultation measurements have been widely used to estimate global planetary boundary layer heights (*H*) using the minimum refractivity gradient method. This method is directly tested here using radiosonde data in China and is found to overestimate summer daytime *H* over land primarily in the presence of multi-inversions in the lower troposphere. This deficiency is largely reduced by adding a constraint with lifting condensation level (LCL) in the derivation of *H*, particularly for LCL < 2 km (usually over humid regions). The primary reason is that our new method effectively avoids estimating *H* near the strong inversion corresponding to the minimum refractivity gradient in the free atmosphere. Applying our new method to the GPS radio occultation data, with LCL derived from surface automatic weather stations, yields more reasonable daytime variation and spatial distribution of *H* over land in China as compared to the ERA5 reanalysis and radiosonde data.

Plain Language Summary The radio signals from Global Positioning System (GPS) satellites have been widely used to estimate global planetary boundary layer heights (*H*) by computing the minimum refractivity variation with height. This method is directly tested here using radiosonde data in China and is found to overestimate summer daytime *H* over land primarily in the presence of multi-inversions (where air temperature increases with height) in the lower troposphere. We use a new method to largely reduce this deficiency by combining the original method with lifting condensation level (LCL) in the derivation of *H*, particularly for LCL < 2 km (usually over humid regions). LCL is the level at which a parcel becomes saturated, representing a reasonable estimate of cloud base height. Our new method effectively avoids the misidentification of *H* near the top of deep clouds. We then apply our method to the GPS satellite data, with LCL derived from surface automatic weather stations. The new results show more reasonable daytime variation and spatial distribution of *H* over land in China as compared to the radiosonde observations and ERA5 reanalysis that makes consistent use of observational data from surface, aircraft, and satellite measurements.

1. Introduction

The planetary boundary layer (PBL) is the lowest part of the troposphere that is directly influenced by the Earth's surface (Garratt, 1992). The PBL processes play significant roles in modulating the exchange of momentum, heat, moisture, gases, and aerosols between the Earth's surface and the free troposphere (Hu et al., 2014; Miao et al., 2015). The PBL height (*H*) is a crucial parameter that can be used to describe much of the diurnal, synoptic, and climatological processes associated with the PBL in a given region, including its cloud characterization and connections between the surface and free troposphere (Ao et al., 2012). It is crucial to accurately estimate *H* through in situ and remote sensing observations, so that the temporal and spatial variations of *H* can be extensively assessed and analyzed at a regional or national scale.

Several ground-based remote sensing instruments (e.g., ceilometer, lidar, sodar, radio acoustic sounding system, and wind profiling radar) have been used to estimate *H*, which effectively complement the limited spatial and temporal sampling of radionsonde observations (Emeis et al., 2004; Liu et al., 2020; Seibert et al., 2000; Zhang et al., 2016). Furthermore, the advent of GPS radio occultation (GPSRO) technique offers global PBL sensing with high vertical resolution (~100 m) and all-weather sounding capability. Numerous studies have demonstrated the advantage of using GPSRO to detect *H* (e.g., Anthes et al., 2008; Ao et al., 2012; Ratnam & Basha, 2010; Sokolovskiy et al., 2006). The *H* estimation with the widely used minimum refractivity gradient method from

GPSRO data performs well when the sharp gradient is present across the transition from PBL to the free troposphere (Ao et al., 2012; Chan & Wood, 2013; P. Guo et al., 2011), specifically over the subtropical ocean characterized by strong subsidence (Ho et al., 2015; Xie et al., 2012). Because the local minimum refractivity gradient at the top of thick clouds (e.g., deep convection over the Inter Tropical Convergence Zone and mid- and high-latitude land regions) is sometimes less than that at the PBL top, the former would be incorrectly regarded as H using the gradient method.

In order to improve the robustness of H detection from GPSRO data, Chan and Wood (2013) added extra constraints to estimate H for sharp-gradient topped PBLs only, but this approach excludes 69% of profiles globally. Basha and Ratnam (2009) compared GPSRO and radiosonde data from a tropical station, and confirmed the good correlation between H derived from gradient of refractivity and other traditional parameters (e.g., potential temperature, virtual potential temperature, mixing ratio). Basha et al. (2019) estimated H from both GPSRO and radiosonde data by using wavelet covariance transform method, and also showed an overall good correlation with relatively small bias (<0.5 km in most cases). In contrast, Basha et al. (2019) demonstrated that GPSRO overestimates H by around 0.9 km compared to the ERA-interim reanalysis data in most of the regions and in all the seasons.

Seidel et al. (2010) discussed the difference and uncertainties in the H estimation by different methods using radiosonde profiles, and showed that the minimum refractivity gradient method significantly overestimates H compared to the parcel method (Seibert et al., 2000). Seidel et al. (2012) further confirmed that the bulk Richardson number method is most suitable to estimate the stable and convective boundary layer height in the radiosonde data, and has also been widely used in weather and climate models and global reanalysis. Gu et al. (2020) showed the poor correlation and large bias between the GPSRO H based on the gradient method and the radiosonde H based on the bulk Richardson number method over land.

Zeng et al. (2004) proposed a method for determining H in radiosonde profile under both cloudy and clear sky conditions by incorporating cloud base height and cloud top height information. They pointed out that the top of a cloud layer thicker than subcloud mixed layer depth and decoupled cloud in free atmosphere generally contains a significant inversion and humidity gradient, which should not be considered as the PBL height. However, since the cloud base height is not easily obtainable, especially for GPSRO data, we propose to use the lifting condensation level (LCL) to approximate the cloud base height and constrain the original refractivity gradient method in GPSRO H estimation. We will test the new method along with the original gradient method using the radiosonde data over China and then evaluate the GPSRO H estimates using the two methods against the radiosonde H data computed using the bulk Richardson number method.

2. Data and Method

In this study, we focus on the daytime H over China by using radiosonde data from 120 China Meteorological Administration operational stations at 2:00 p.m. Beijing time (BT) during summer (June–August) of 2011–2018 (J. Guo et al., 2016; Zhang et al., 2018). In addition, we use in situ hourly measurements of temperature (T) and relative humidity (RH) at 2 m height and surface pressure data from 2,684 China automatic weather stations (AWS), which are provided by China National Meteorological Information Center. We also use the GPSRO refractivity profiles with moisture information (called wetPrf) from surface up to 5 km above surface during the same period. All the GPSRO data used in this study are from the Constellation Observing System for the Meteorology, Ionosphere, and Climate (COSMIC) satellite mission. In addition, we use the 3-hourly $0.25° \times 0.25°$ ERA5 reanalysis H product (H_{EC}) in summer (June–August) from 2011 to 2018 (Hersbach et al., 2020).

For radiosonde data, we use three methods (bulk Richardson number, minimum refractivity gradient, and a new method) to calculate the corresponding PBL heights (H_{obs}, H_{ori}, and H_{new}). The radiosonde data were smoothed by using a 1–2–1 smoother, that is, the smoothed value at a given level as the weighted sum of the values at a lower level multiplied by 25%, at the level of interest multiplied by 50%, and at a higher level multiplied by 25% (Zeng et al., 2004). For GPSRO data, we only calculate H_{ori} and H_{new}. Because many GPSRO miss the data close to the surface, for the purpose of getting valid samples for H estimation, especially in a region of high topographic relief (mid-western China), we only select the refractivity profile extending below 1.0 km above the surface and the number of missing data less than 30. As this study focuses on the H over land during the daytime in summer which is generally higher than 1 km, especially in mid-western China, selecting 1.0 km rather than 0.5 km as the threshold has little influence on the results of H from GPSRO.

The bulk Richardson number (Ri) method proposed by Vogelezang and Holtslag (1996) is one of the most widely adopted methods to define H from radiosonde, model, and reanalysis data. The H_{obs} from radiosondes is estimated as the height (starting from near-surface) where Ri reaches the critical value, for example, $Ri_c = 0.25$. The Ri is the ratio of turbulence associated with buoyancy to that associated with mechanical shear, such as:

$$\mathrm{Ri}(z) = \frac{(g/\theta_{vs})(\theta_{vz} - \theta_{vs})(z - z_s)}{(u_z - u_s)^2 + (v_z - v_s)^2 + (bu_*^2)}, \tag{1}$$

where z is height, and s denotes the surface (or the height of the first model layer above surface in models or reanalysis data), g is the acceleration of gravity, θ_v is virtual potential temperature, u and v are component wind speeds, b is a constant, and u_* is the surface friction velocity. Here, we ignore the term bu_* due to the much smaller magnitude compared with bulk wind shear term in the denominator (Vogelezang & Holtslag, 1996). Further, measurements at the lowest level from the radiosonde data are used to compute u_s, v_s, and θ_{vs}.

For the ERA5 reanalysis, the PBL height (H_{EC}) is diagnosed as the lowest level at which Ri reaches the critical value of 0.25 (Seidel et al., 2012; Vogelezang & Holtslag, 1996).

The microwave refractivity N is computed from (Smith & Weintraub, 1953):

$$N = a_1 \frac{P}{T} + a_2 \frac{P_w}{T^2}, \tag{2}$$

where T is the temperature (K), P is the total pressure (hPa), and P_w is the water vapor partial pressure (hPa), with constants $a_1 = 77.6$ K/hPa, $a_2 = 3.73 \times 10^5$ K^2/hPa.

Based on Equation 2, Ao et al. (2012) pointed out that the vertical refractivity gradient, $N' \equiv \mathrm{d}N/\mathrm{d}z$, can be written as:

$$N' = a_1 \frac{1}{T} P' - \left(a_1 \frac{P}{T^2} + 2a_2 \frac{P_w}{T^3} \right) T' + a_2 \frac{P_w'}{T^2} \equiv N_P' + N_T' + N_w', \tag{3}$$

where the last three terms correspond to the contributions to the refractivity gradients from P, T, and P_w, respectively. For typical conditions (Figure 1), N_w' varies more with height than N_p' and N_T', thus the heights of local minimum N' mainly depend on N_w'. Only at very low temperatures situation, such as the polar region, when P_w is low, N_T' contributes most to N' (Chan & Wood, 2013). H_{ori} is estimated as the height of the minimum N'. This method is appropriate when a sharp gradient exists at PBL top, but it may not work well if there are multiple inversions that correspond to multilocal minimum refractivity gradients in the atmosphere (e.g., Figure 1). Our new method intends to address this issue.

Zeng et al. (2004) proposed a method for determining H in radiosonde profile under both cloudy and clear sky conditions by incorporating cloud base height and cloud top height information. They pointed out that the top of a cloud layer thicker than subcloud mixed layer depth and decoupled cloud in free atmosphere should not be considered as H. Motivated by that study, here we propose a new method to calculate H with the refractivity profile constrained by the LCL.

In general, LCL is a function of air temperature (T), RH, and surface pressure (Romps, 2017). We use the LCL constraint to exclude H_{ori} identified by the minimum refractivity gradient method when H_{ori} is greater by more than 1 km than LCL, or when the difference of (H_{ori}–LCL) is greater than LCL. For the first condition, H_{ori} often corresponds to the height of local minimum N' (e.g., the top of clouds) in free atmosphere. For the second condition, if cloud exists from LCL to H_{ori}, the cloud depth is deeper than the depth of subcloud mixing layer, and in this case H_{ori} corresponds to the top of deep clouds defined in Zeng et al. (2004).

The LCL for individual GPSRO profile is calculated based on the surface air temperature, RH and pressure from collocated AWS data. For radiosonde data, we use the values at the lowest level from the raw data to calculate LCL.

The detail of the new method for computing the PBL height (H_{new}) is as follows:

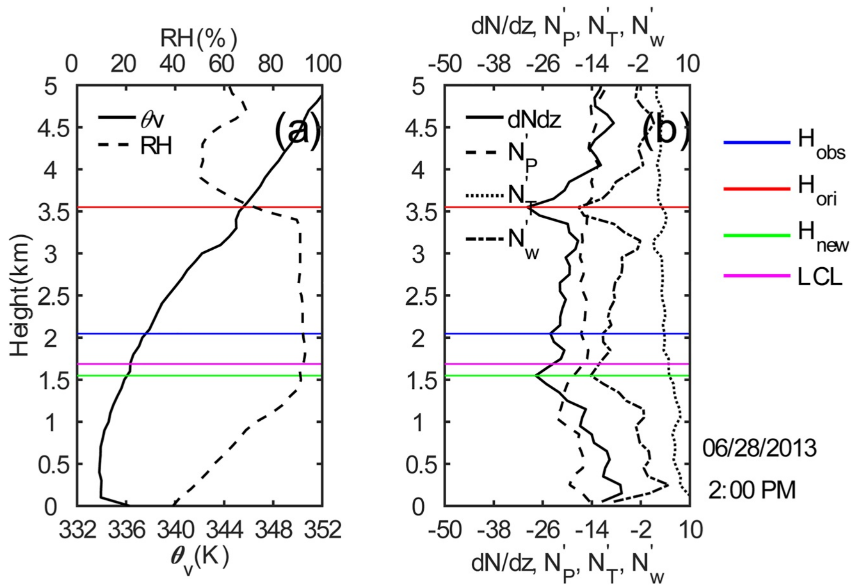

Figure 1. (a) The vertical profiles of radiosonde virtual potential temperature (θ_v) and relative humidity (RH) on June 28, 2013 at 2:00 p.m. Beijing time (BT) in Naqu (Longitude: 92.07°E, latitude: 31.48°N, elevation: 4,508 m), China. (b) Vertical profiles of refractivity gradient (N-unit/km) and the separate contributions from pressure, temperature, and water vapor gradients. Horizontal lines denote H_{obs} (blue), H_{ori} (red), H_{new} (green), and LCL (pink), respectively. Note that the minimum refractivity gradient at this high elevation site in panel (b) is much smaller in magnitude than those at low elevation sites.

1. Identify each of the local minimum refractivity gradients, $\mathrm{d}N/\mathrm{d}z_i$, from bottom to 5 km above the surface (as H can be greater than 4 km over deserts) and its corresponding height h_i ($i = 1, 2,\ldots, m$, with m representing the total number of such local minimum gradients)
2. Select the minimum value of $\mathrm{d}N/\mathrm{d}z_i$, denoted as $\mathrm{d}N/\mathrm{d}z_j$, and the corresponding h_j ($1 \le j \le m$)
3. If h_j–LCL < 1 km and h_j–LCL < LCL, $H_{new} = h_j$ (and no further iteration is needed)
4. If h_j–LCL > 1 km or h_j–LCL > LCL, we select the minimum value of $\mathrm{d}N/\mathrm{d}z_i$ (excluding $\mathrm{d}N/\mathrm{d}z_j$) below the height of h_j, denoted as $\mathrm{d}N/\mathrm{d}z_k$ ($1 \le k < j$) and its corresponding height is h_k. Then repeat steps (c) and (d) by assigning k to j

These steps ensure the exclusion of the misidentified H from gradient method (H_{ori}) in the free troposphere. Therefore, H_{new} is always less than or equal to H_{ori}. In other words, the new method only improves results when H_{ori} overestimates the PBL height.

3. Results

3.1. Radiosonde Data Analysis

To test our new method, we first compute N from Equation 2 using the radiosonde data. Then we compute H_{ori} and H_{new} from N and compare them against H_{obs} computed from the radiosonde data directly, using the methods discussed in Section 2. At 2:00 p.m. BT, the median differences of (H_{ori}–H_{obs}) and (H_{new}–H_{obs}) at radiosonde sites in northern China are similar, while median differences of (H_{ori}–H_{obs}) are slightly larger than those of (H_{new}–H_{obs}) in south China (Figures 2a and 2b). The interquartile ranges (IQRs) of (H_{new}–H_{obs}) (mean IQR = 0.75 km) are significantly less than those of (H_{ori}–H_{obs}) (mean IQR = 1.04 km) (Figures 2c and 2d). Further, the correlation coefficients (R) between H_{new} and H_{obs} (mean R = 0.65) at individual radiosonde sites are generally higher by more than 50% than those between H_{ori} and H_{obs} (mean R = 0.37) (Figures 2e and 2f). Consistent with the results in Figures 2c and 2d, the root mean square differences (RMSDs) of (H_{new}–H_{obs}) (mean RMSD = 0.66 km) are smaller than those of (H_{ori}–H_{obs}) (mean RMSD = 1.07 km) (Figure S1 in Supporting Information S1).

To better understand the improved performance of H_{new} over H_{ori}, we have carefully analyzed individual radiosonde profiles and identified the presence of multi-inversions in the lower troposphere as the primary reason. As an example, Figure 1b shows the presence of multi-inversions in the lower troposphere. The H_{ori} based on

10.1029/2021GL096304

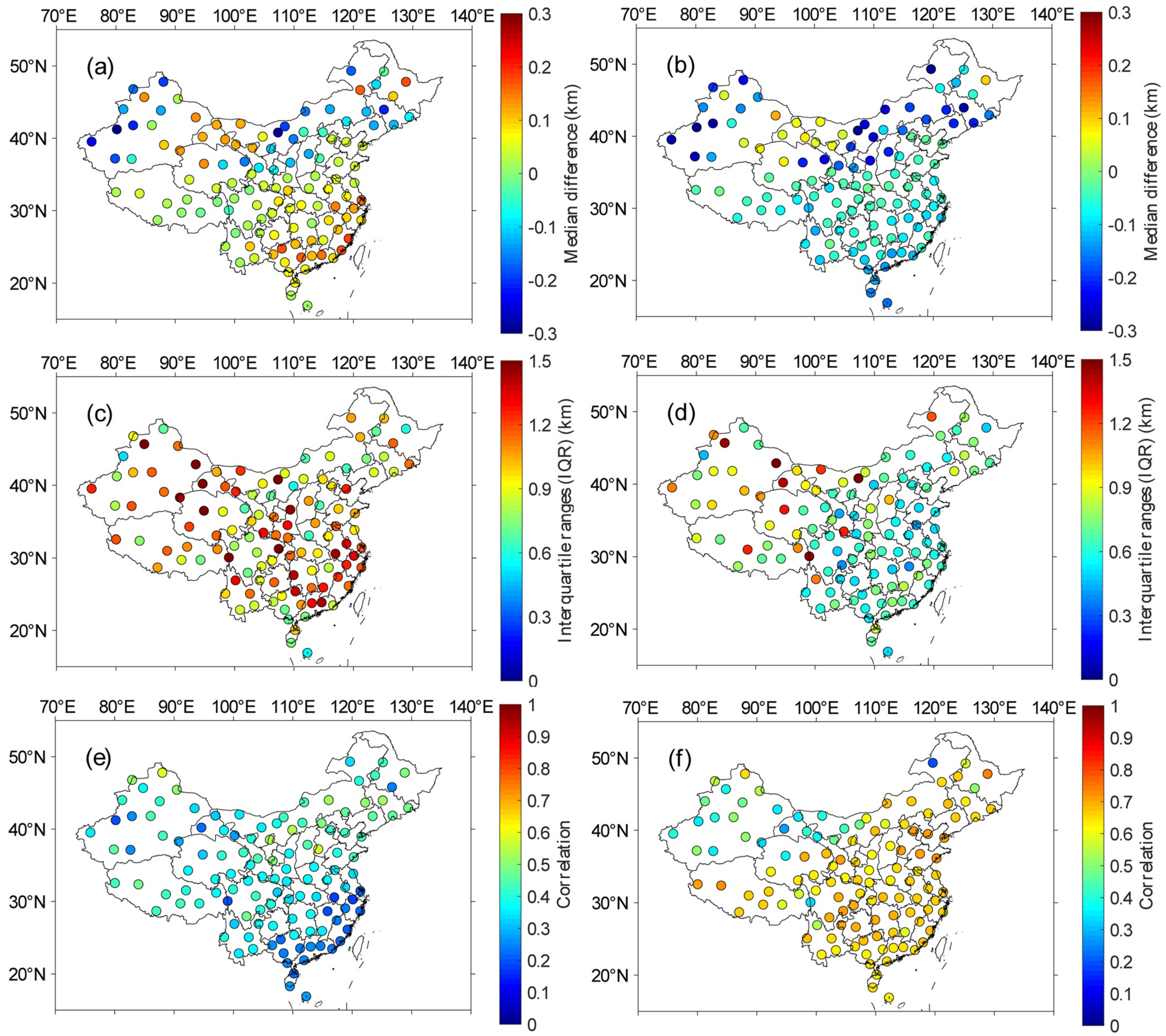

Figure 2. The median differences of (a) H_{ori}–H_{obs} and (b) H_{new}–H_{obs} for each radiosonde site at 2:00 p.m. BT from June to August (2011–2018) in China; (c and d) are the corresponding interquartile range (IQR); and (e and f) show the correlation coefficient of (H_{obs} and H_{ori}), and (H_{obs} and H_{new}) at each radionsonde site, respectively.

refractivity gradient method is 3.5 km, which is about 1.5 km higher than H_{obs} (~2.0 km). With the LCL of ~1.7 km, (H_{ori}–LCL) of 1.8 km is greater than LCL, and our new method identifies the next local minimum refractivity gradient at H_{new} = 1.6 km, which is much closer to H_{obs}. Sun et al. (2010) showed that Chinese radiosondes underestimate RH by about 10% at high elevation stations, thus RH > 90% could imply likely cloud presence in the selected radiosonde over the Tibet Plateau (Figure 1). The high cloud fraction of the low cloud (90%) from the surface observation also confirms this speculation. Thus, the RH profile in Figure 1a shows a cloud thickness of ~1.9 km with the cloud base and top at about 1.6 and 3.5 km, respectively. Therefore, H_{ori} represents the cloud top, while LCL is close to the cloud base. According to the method of Zeng et al. (2004) for H estimation, the cloud thickness of 1.9 km is greater than cloud base (~1.6 km), and the cloud top (~3.5 km) in the free atmosphere (i.e., H_{ori}) should not be considered as the PBL height. In contrast, H_{new} of 1.6 km is a better representation of H_{obs}.

One question on using H_{obs} as reference is how the above test results are affected by the uncertainty in computing $H_{obs.}$ Previous studies indicated that H_{obs} is not very sensitive to the critical Richardson number

10.1029/2021GL096304

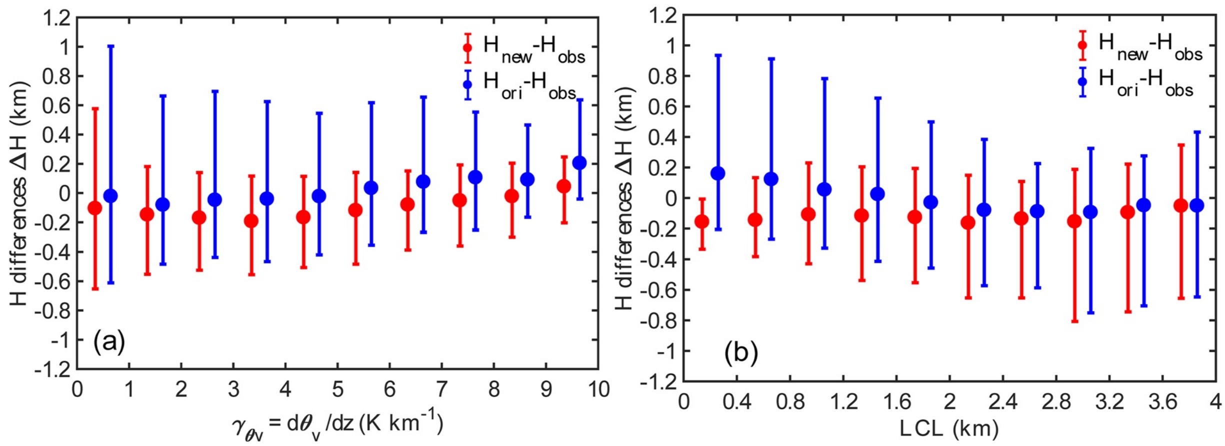

Figure 3. The variations of H differences (ΔH) with (a) γ_{θ_v} and (b) LCL using all the samples at 120 radiosonde sites. The red and blue circles denote median values for H_{new}–H_{obs} and H_{ori}–H_{obs}, respectively. The error bars denote the 25th and 75th percentiles, respectively.

(Seidel et al., 2012; J. Guo et al., 2016). In addition, our results show that H_{obs} is not sensitive to the increasing of vertical resolution from 100 to 25 m (Figure not shown). In fact, the uncertainty of H_{obs} mainly depends on the value of virtual potential temperature in surface layer (θ_{vs}) and the gradient of θ_v ($\gamma_{\theta_v} = d\theta_v/dz$) above PBL. Stull (1988) pointed out that the PBL height is usually defined at the center of entrainment zone, and the uncertainty of H_{obs} generally increases with the increase of the depth of entrainment zone (or the decrease of γ_{θ_v}). Therefore, the large IQRs of ($H_{ori}-H_{obs}$) and ($H_{new}-H_{obs}$) at very small γ_{θ_v} values (e.g., between 0 and 1 K km^{-1}, occurring for less than 5% of the time [Figure S2a in Supporting Information S1]) in Figure 3a could be partly contributed by H_{obs} uncertainties, while the smaller IQRs of ($H_{new}-H_{obs}$) than those of ($H_{ori}-H_{obs}$) at larger γ_{θ_v} values (e.g., >1 K km^{-1}) are not much affected by H_{obs} uncertainties. Furthermore, the IQR differences between ($H_{ori}-H_{obs}$) and ($H_{new}-H_{obs}$) are mainly contributed by the upper limit (i.e., the 75th percentile) (Figure 3a), while the differences in the median or the lower limit are quite small. Similarly, the much smaller RMSDs of ($H_{new}-H_{obs}$) than those of (H_{ori}–H_{obs}) at larger γ_{θ_v} values (e.g., >1 K km^{-1}) are not much affected by H_{obs} uncertainties in Figures S2a and S2c in Supporting Information S1. These results indicate that H_{new} improves the results primarily when H_{ori} overestimates the PBL height.

Because LCL is used in computing H_{new}, it would be interesting to evaluate the dependence of (H_{ori}–H_{obs}) and (H_{new}–H_{obs}) on LCL. While the IQRs of (H_{ori}–H_{obs}) and (H_{new}–H_{obs}) are similar for LCL > 2 km (Figure 3b), those of (H_{new}–H_{obs}) are smaller for LCL < 2 km. Further, the IQRs of (H_{new}–H_{obs}) [or (H_{ori}–H_{obs})] decreases (or increases) with the decreasing LCL for LCL < 2 km (Figure 3b). Similarly, the smaller RMSDs of (H_{new}–H_{obs}) than those of (H_{ori}–H_{obs}) occur primarily for LCL < 2 km (Figures S2b and S2d in Supporting Information S1).

Over arid regions with higher LCL, the criterion (c) of the new method in Section 2 is much harder to meet. Thus the improvement of adding a constraint with LCL is limited. The occurrence of sharp gradients (in N or P_w) at PBL top in arid regions is also less frequent than in humid regions. There are often multiple inversions that correspond to multilocal minimum refractivity gradients with values close to each other bellow LCL (even within the PBL) in arid regions (figure not shown). For these cases, the new method does not improve the results either. Furthermore, the weak inversion layer of θ_v above PBL ($\gamma_{\theta_v} < 2$ K km^{-1}) occurs more frequently (23%) in the relatively dry western China (75°E−100°E, 25°N–50°N) than in the relatively humid eastern China (13%). This increases the uncertainty of H_{obs}, partially contributing to the relatively large IQRs (Figure 2a) and RMSDs (Figures S2a and S2c in Supporting Information S1) of (H_{new}–H_{obs}) and (H_{ori}–H_{obs}) at $\gamma_{\theta_v} < 2$ K km^{-1}.

3.2. GPSRO Data Analysis

Next, we apply our new method to the 8-year satellite GPSRO data (June–August, 2011–2018) over China to compute H_{new}. We then bin the daytime results into 2° (latitude) × 2° (longitude) grids within 1.5 hr at three different times (11:00 a.m., 2:00 p.m., and 5:00 p.m. BT). Figures 4d–4f show that H_{new} increases from the humid

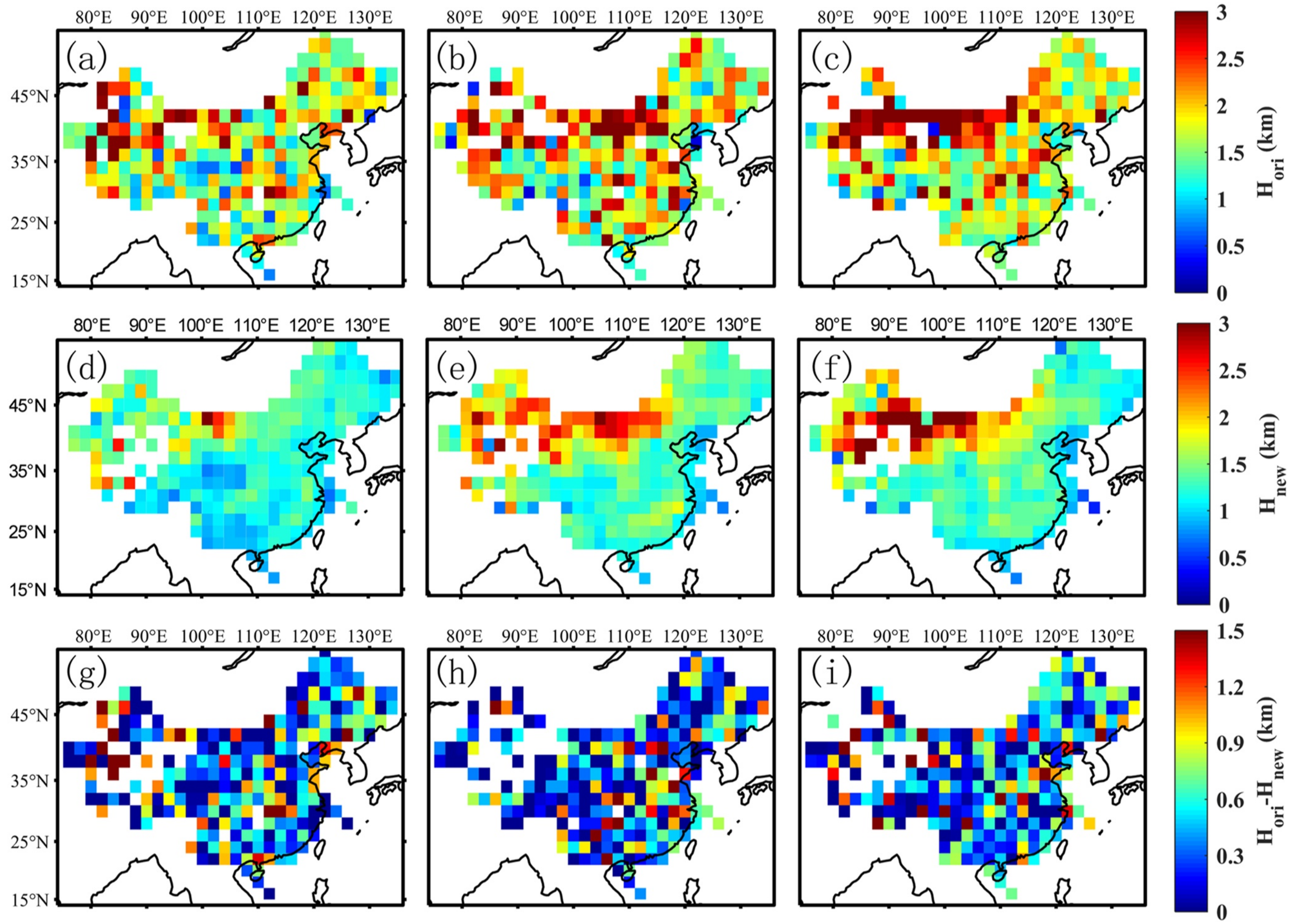

Figure 4. The mean H_{ori} derived from GPSRO data at three Beijing times: (a) 11:00 a.m. ± 1.5 hr, (b) 2:00 p.m. ± 1.5 hr, and (c) 5:00 p.m. ± 1.5 hr from June to August (2011–2018) in China. (d–f) and (g–i) are the same as (a–c) but for the mean H_{new} and (H_{ori}–H_{new}), respectively. Missing data are shaded in white color.

south to the arid northwest of China, which is consistent with the spatial distribution of H_{obs} from radiosondes and H_{EC} from ERA5 reanalysis (Figure S3 in Supporting Information S1).

The mean H_{EC} and the collocated mean H_{new} at 2° × 2° grids at 2:00 p.m. BT over China show a high spatial correlation ($R = 0.72$ with RMSD = 0.39 km), which is much higher than that between H_{EC} and H_{ori} ($R = 0.39$ with RMSD = 0.83 km). Further, Figures 4d–4f show that H_{new} gradually increases from late morning to afternoon. For instance, the H_{new} values are about 1.67 km, 2.24 and 2.63 km in northwestern China (90°E−100°E, 38°N–44°N) at 11:00 a.m., 2:00 p.m., and 5:00 p.m. BT (i.e., at 9:30 a.m., 12:30 p.m., and 3:30 p.m. local time at 95°E), respectively.

Our analysis using the radiosonde data in Section 3.1 indicates that the new method improves the results when H_{ori} overestimates the PBL height and the median differences between H_{new} and H_{ori} are small. Indeed the median (H_{ori}–H_{new}) differences are also small using the GPSRO data (Figure not shown). The (H_{ori}–H_{new}) differences are positive over all areas (Figure 4), as expected from the new method (see the discussion at the end of Section 2). For instance, in eastern China (110°E−120°E, 26°N–36°N) at 2:00 p.m. BT, the mean H_{new} is 1.32 km and (H_{ori}–H_{new}) is 0.58 km. Figure 4 also shows that the spatial pattern of H_{new} is smooth, while that of H_{ori} is quite noisy, leading to the lack of spatial pattern of (H_{ori}–H_{new}).

To directly evaluate H_{new} and H_{ori} from GPSRO (with a horizontal resolution of about 200 km) using H_{obs} from radiosonde data over China, we identify the collocated GPSRO data to be within 1.5 hr difference and within 200 km from AWS sites with radiosonde data during summer (June–August) of 2011–2018. There are 227 collocated cases at 2:00 p.m. BT and the results are shown in Figure S4 in Supporting Information S1. The H_{new}

derived from the GPSRO data significantly improves its correlation ($R = 0.47$) with H_{obs} from radiosondes (Figure S4b in Supporting Information S1) compared with H_{ori} (with the correlation $R = 0.26$; Figure S4a in Supporting Information S1). While the median (H_{ori}–H_{obs}) is quite similar to (H_{new}–H_{obs}), the upper limit of IQR (or the 75th percentile) decreases from 1.0 km for (H_{ori}–H_{obs}) to 0.3 km for (H_{new}–H_{obs}), consistent with the results in Figure 3 (using radiosonde data alone).

4. Conclusions and Discussion

The refractivity gradient method has been widely used to derive global PBL height (H_{ori}) from the GPSRO satellite data. We have directly tested this method using the refractivity computed from radiosonde data over China. It is found that H_{ori} could significantly overestimate the PBL height in the presence of multi-inversions that correspond to multilocal minimum refractivity gradients in the lower troposphere. To alleviate this issue, we combine the original refractivity gradient method with an LCL constraint to estimate the PBL height (H_{new}). In general, the LCL can be computed from the radiosonde data at the lowest level or from surface measurements at conventional weather stations. Based on the analysis of 8 yr summertime radiosonde data at 2:00 p.m. BT in China, the new method effectively improves the estimation of the daytime PBL height over humid regions with LCL < 2 km.

We have then applied the new method to the satellite GPSRO data over China. Consistent with the results from the ERA5 reanalysis, the daytime H_{new} in summer shows the increase of the PBL height from the humid south to the arid northwest over China. Comparison of H_{new} and H_{ori} from GPSRO with H_{obs} from collocated radiosonde sites shows that the new method increases the correlation with H_{obs} and improves the results when H_{ori} overestimates the PBL height in China.

However, our new method does not improve the results over arid regions with LCL > 2 km. Sometimes the new method may underestimate the PBL height more than the original method, as indicated by the slightly worse 25th percentile of (H_{new}–H_{obs}) than (H_{ori}–H_{obs}) in Figures 3 and Figure S4 in Supporting Information S1. In addition, estimating the height of nighttime stable boundary layer over land with GPSRO data remains very challenging due to the limited vertical resolution and penetration of sounding near the surface. For this reason, both the new and original methods likely capture the top of residual layer (from daytime) at night and significantly overestimate the stable boundary layer height. These issues warrant future investigation.

Data Availability Statement

The GPSRO data from the Constellation Observing System for the Meteorology, Ionosphere, and Climate (COSMIC) satellite mission are downloaded from the UCAR COSMIC Data Analysis and Archive Center (CDDAC, https://data.cosmic.ucar.edu/gnss-ro/cosmic1/). The radiosonde data and in situ measurements are from the China National Meteorological Information Center (http://data.cma.cn/en), the users need to register an account, and then refer to the introductions in link http://data.cma.cn/en/?r=article/getLeft/id/343/keyIndex/30. ERA5 reanalysis data are from European Centre for Medium-Range Weather Forecasts (https://cds.climate.copernicus.eu/cdsapp#!/dataset/reanalysis-era5-single-levels?tab=form), and the processed data can be obtained in https://www.scidb.cn/en/s/qqyqMb.

Acknowledgments
The authors thank two reviewers for helpful comments and suggestions that lead to improved discussion of results and corrected Figure S4 in Supporting Information S1. Wang and Xu are supported by the National Natural Science Foundation for Young Scientists of China (grant No. 41805006), National Natural Science Foundation of China (grant No. 91837310), and the Second Tibetan Plateau Scientific Expedition and Research (STEP) program (grant No. 2019QZKK0105). Zeng is supported by the U.S. Department of Energy SciDAC Program.

References

Anthes, R. A., Bernhardt, P. A., Chen, Y., Cucurull, L., Dymond, K. F., Ector, D., et al. (2008). The COSMIC/FORMOSAT-3 mission: Early results. *Bulletin of the American Meteorological Society*, *89*, 313–334. https://doi.org/10.1175/BAMS-89-3-313

Ao, C. O., Waliser, D. E., Chan, S. K., Li, J.-L., Tian, B., Xie, F., & Mannucci, A. J. (2012). Planetary boundary layer heights from GPS radio occultation refractivity and humidity profiles. *Journal of Geophysical Research: Atmospheres*, *117*(D16), 16117. https://doi.org/10.1029/2012JD017598

Basha, G., Kishore, P., Ratnam, M. V., Ravindra Babu, S., Velicogna, I., Jiang, J. H., & Ao, C. O. (2019). Global climatology of planetary boundary layer top obtained from multi-satellite GPS RO observations. *Climate Dynamics*, *52*, 2385–2398. https://doi.org/10.1007/s00382-018-4269-1

Basha, G., & Ratnam, M. V. (2009). Identification of atmospheric boundary layer height over a tropical station using high-resolution radiosonde refractivity profiles: Comparison with GPS radio occultation measurements. *Journal of Geophysical Research: Atmospheres*, *114*(D16). https://doi.org/10.1029/2008JD011692

Chan, K. M., & Wood, R. (2013). The seasonal cycle of planetary boundary layer depth determined using cosmic radio occultation data. *Journal of Geophysical Research: Atmospheres*, *118*(22), 12422–12434. https://doi.org/10.1002/2013JD020147

Emeis, S., Münkel, C., Vogt, S., Müller, W. J., & Schäfer, K. (2004). Atmospheric boundary-layer structure from simultaneous SODAR, RASS, and ceilometer measurements. *Atmospheric Environment*, *38*, 273–286. https://doi.org/10.1016/j.atmosenv.2003.09.054

Garratt, J. R. (1992). *The atmospheric boundary layer* (p. 316). Cambridge University Press.

Gu, J., Zhang, Y., Yang, N., & Wang, R. (2020). Comparisons in the global planetary boundary layer height obtained from COSMIC radio occultation, radiosonde, and reanalysis data. *Atmospheric and Oceanic Science Letters*, *14*(3), 100018. https://doi.org/10.1016/j.aosl.2020.100018

Guo, J., Miao, Y., Zhang, Y., Liu, H., Li, Z., Zhang, W., et al. (2016). The climatology of planetary boundary layer height in China derived from radiosonde and reanalysis data. *Atmospheric Chemistry and Physics*, *16*, 13309–13319. https://doi.org/10.5194/acp-16-13309-2016

Guo, P., Kuo, Y. H., Sokolovskiy, S. V., & Lenschow, D. H. (2011). Estimating atmospheric boundary layer depth using COSMIC radio occultation data. *Journal of the Atmospheric Sciences*, *68*, 1703–1713. https://doi.org/10.1175/2011JAS3612.1

Hersbach, H., Bell, B., Berrisford, P., Hirahara, S., Horányi, A., Muñoz-Sabater, J., et al. (2020). The ERA5 global reanalysis. *Quarterly Journal of the Royal Meteorological Society*, *146*, 1999–2049. https://doi.org/10.1002/qj.3803

Ho, S., Peng, L., Anthes, R. A., Kuo, Y., & Lin, H. C. (2015). Marine boundary layer heights and their longitudinal, diurnal, and interseasonal variability in the Southeastern Pacific using COSMIC, CALIOP, and radiosonde data. *Journal of Climate*, *28*(7), 2856–2872. https://doi.org/10.1175/JCLI-D-14-00238.1

Hu, X. M., Ma, Z. Q., Lin, W., Zhang, H., Hu, J., Ying, W., et al. (2014). Impact of the loess plateau on the atmospheric boundary layer structure and air quality in the north China plain: A case study. *Science of the Total Environment*, *499*, 228–237. https://doi.org/10.1016/j.scitotenv.2014.08.053

Liu, B., Guo, J., Gong, W., Shi, Y., & Jin, S. (2020). Boundary layer height as estimated from Radar wind profilers in four cities in China: Relative contributions from aerosols and surface features. *Remote Sensing*, *12*, 1657. https://doi.org/10.3390/rs12101657

Miao, Y., Hu, X. M., Liu, S., Qian, T., Xue, M., Zheng, Y., & Wang, S. (2015). Seasonal variation of local atmospheric circulations and boundary layer structure in the Beijing-Tianjin-Hebei region and implications for air quality. *Journal of Advances in Modeling Earth Systems*, *7*, 1602–1626. https://doi.org/10.1002/2015MS000522

Ratnam, M. V., & Basha, S. G. (2010). A robust method to determine global distribution of atmospheric boundary layer top from cosmic GPS RO measurements. *Atmospheric Science Letters*, *11*(3), 216–222. https://doi.org/10.1002/asl.277

Romps, D. M. (2017). Exact expression for the lifting condensation level. *Journal of the Atmospheric Sciences*, *74*, 3891–3900. https://doi.org/10.1175/JAS-D-17-0102.1

Seibert, P., Beyrich, F., Gryning, S. E., Joffre, S., Rasumussen, A., & Tercier, P. (2000). Review and intercomparison of operational methods for the determination of the mixing height. *Atmospheric Environment*, *34*, 1001–1027. https://doi.org/10.1016/S1352-2310(99)00349-0

Seidel, D. J., Ao, C. O., & Li, K. (2010). Estimating climatological planetary boundary layer heights from radiosonde observations: Comparison of methods and uncertainty analysis. *Journal of Geophysical Research: Atmospheres*, *115*, D16113. https://doi.org/10.1029/2009JD013680

Seidel, D. J., Zhang, Y., Beljaars, A., Golaz, J.-C., Jacobson, A. R., & Medeiros, B. (2012). Climatology of the planetary boundary layer over the continental United States and Europe. *Journal of Geophysical Research: Atmospheres*, *117*, D17106. https://doi.org/10.1029/2012JD018143

Smith, E. K., & Weintraub, S. (1953). The constants in the equation for atmospheric refractive index at radio frequencies. *Proceedings of the IEEE*, *41*, 1035–1037. https://doi.org/10.1109/JRPROC.1953.274297

Sokolovskiy, S., Kuo, Y.-H., Rocken, C., Schreiner, W. S., Hunt, D., & Anthes, R. A. (2006). Monitoring the atmospheric boundary layer by GPS radio occultation signals recorded in the open-loop mode. *Geophysical Research Letters*, *33*, L12813. https://doi.org/10.1029/2006GL025955

Stull, R. B. (1988). *An introduction to boundary layer meteorology* (p. 666). Kluwer Academic Publishers.

Sun, B., Reale, A., Seidel, D. J., & Hunt, D. C. (2010). Comparing radiosonde and cosmic atmospheric profile data to quantify differences among radiosonde types and the effects of imperfect collocation on comparison statistics. *Journal of Geophysical Research: Atmospheres*, *115*(D23). https://doi.org/10.1029/2010JD014457

Vogelezang, D., & Holtslag, A. (1996). Evaluation and model impacts of alternative boundary-layer height formulations. *Boundary-Layer Meteorology*, *81*(3–4), 245–269. https://doi.org/10.1007/BF02430331

Xie, F., Wu, D. L., Ao, C. O., Mannucci, A. J., & Kursinski, E. R. (2012). Advances and limitations of atmospheric boundary layer observations with GPS occultation over southeast Pacific Ocean. *Atmospheric Chemistry and Physics*, *12*, 903–918. https://doi.org/10.5194/acp-12-903-2012

Zeng, X., Brunke, M. A., Zhou, M., Fairall, C., Bond, N. A., & Lenschow, D. H. (2004). Marine atmospheric boundary layer height over the eastern pacific: Data analysis and model evaluation. *Journal of Climate*, *17*(21), 4159–4170. https://doi.org/10.1175/JCLI3190.1

Zhang, W., Guo, J., Miao, Y., Liu, H., Song, Y., Fang, Z., et al. (2018). On the summertime planetary boundary layer with different thermodynamic stability in China: A radiosonde perspective. *Journal of Climate*, *31*(4), 1451–1465. https://doi.org/10.1175/JCLI-D-17-0231.1

Zhang, W., Guo, J., Miao, Y., Liu, H., Zhang, Y., Li, Z., & Zhai, P. (2016). Planetary boundary layer height from CALIOP compared to radiosonde over China. *Atmospheric Chemistry and Physics*, *16*, 9951–9963. https://doi.org/10.5194/acp-16-9951-2016